Title	A kicked oscillator as a model of a pulsed MEMS system
Authors(s)	Blokhina, Elena, Feely, Orla
Publication date	2009-01
Publication information	Blokhina, Elena, and Orla Feely. “A Kicked Oscillator as a Model of a Pulsed MEMS System.” World Scientific Publishing, January 2009. https://doi.org/10.1142/S0218127409022828.
Publisher	World Scientific Publishing
Item record/more information	http://hdl.handle.net/10197/3591
Publisher's statement	Electronic version of an article published as International Journal of Bifurcation and Chaos, 10 (1): 187-202 DOI: 10.1142/S0218127409022828 © World Scientific Publishing Company http://www.worldscinet.com/ijbc/19/1901/S0218127409022828.html
Publisher's version (DOI)	10.1142/S0218127409022828

A KICKED OSCILLATOR AS A MODEL OF A PULSED MEMS SYSTEM

ELENA BLOKHINA and ORLA FEELY
School of Electrical, Electronic and Mechanical Engineering,
University College Dublin, Belfield, Dublin 4, Ireland

Received (Day Month Year)
Revised (Day Month Year)

In this paper, we study the behaviour of a MEMS oscillator by applying methods of nonlinear dynamics. We model the system as a kicked damped oscillator and obtain the iterative maps that describe the MEMS system. The dynamics of the maps are studied numerically: we present a study of limit cycles and their rotation numbers and show how the control parameters and initial conditions may affect the output frequencies.

1. Introduction

Microelectromechanical systems (MEMS) are integrated devices that combine electrical and mechanical components [Bao & Wang, 1996]. Resonant sensors are a class of MEMS devices whose applications include the measurement of acceleration, pressure, mass change, etc. Resonant sensors detect the frequency shift of an oscillating mechanical structure or a change in the amplitude of oscillation at resonance in response to an external stimulus [Langdon, 1985; Parsons, 1993].

In this paper, we focus on the pulsed digital MEMS oscillator. This is a new large signal oscillator described in [Dominguez *et al.*, 2003; Dominguez *et al.*, 2005; Dominguez *et al.*, 2007] that utilises a MEMS resonator in a feedback loop of a type well known from the domain of sigma-delta modulation [Norsworthy *et al.*, 1997]. The simple topology of this oscillator is shown in Fig. 1. The position of the MEMS resonator is evaluated at each sampling time, and short force pulses (which can take only two possible values depending on the position of the resonator) are applied to it after a sample clock delay.

MEMS resonators are typically modelled by mass-spring-damping systems, either linear or nonlinear. For instance, the nonlinearity in resonant microbridges leading to additional stiffening known, as the "hard-spring effect", is discussed in [Gui *et al.*, 1998]. Zhang *et al.* [2002] report how nonlinearity affects the behaviour of a resonant MEMS mass sensor under parametric excitation. The nonlinear behaviour of an electrostatically actuated micro-cantilever in a MEMS is presented in [Zhang & Meng, 2005; Zhang &

Meng, 2007], while Palaniapan & Khine [2008] study the dynamics of a nonlinear SOI micromechanical beam resonator. In all of these papers, MEMS resonators of different types have been simplified as a mass-spring-damping system (as shown in Fig. 1), and the corresponding equations, linear or containing a cubic nonlinear term, have been used to model the mechanical part of the MEMS.

Our aim, then, is to study a mechanical oscillator, which can be linear or nonlinear, driven by pulses of a constant frequency with the sign of each pulse depending on the position of the oscillator. This kicked oscillator is a good approximation for the pulsed digital MEMS. In addition, this is quite a common model of nonlinear dynamics and can be studied with its methods and techniques.

Kicked oscillators have been extensively studied as models of many realistic systems (for instance, see [Kuznetsov *et al.*, 2001; Kuznetsov & Tyuryukina, 2003; Kuznetsov *et al.*, 2006; Mudde & Jansz, 2003] and references cited there). Kuznetsov *et al.* [2001] consider a dissipative nonlinear oscillator kicked periodically by pulses of a constant amplitude and sign. They examine 2D and approximate 1D maps and discuss the correspondence between the description provided by the equation and the maps. Mudde & Jansz [2003] present a numerical study of a linear dissipative delta-kicked oscillator where the kicks have a constant frequency and amplitude, but their signs are defined by the sign of the velocity of the oscillator. The model we propose in this paper to simulate the MEMS system under investigation combines some features from both these systems: the oscillator can be linear or nonlinear and it is driven by impulses of different signs.

The aim of this work is to apply the techniques of nonlinear dynamics to study a particular class of MEMS systems and to compare the dynamics with linear and nonlinear resonators. We present a kicked oscillator as a model of the digital pulsed MEMS resonator from [Dominguez *et al.*, 2005] and obtain 2D maps to describe it. We start with the linear resonator, which has been studied in [Teplinsky & Feely, 2008]. We summarise some results of that paper and present them here with some extensions. Then we generalise the problem and consider the nonlinear resonator described by the Duffing equation. We show which additional effects appear due to mechanical nonlinearity and compare the results with those obtained for the linear system. We also discuss the correspondence between the description of the system in terms of the differential equation and the iterative map.

2. Linear resonator

First of all, let us examine the linear case. This system has been studied in [Teplinsky & Feely, 2008] and we present for convenience a summary of the results of that work here, together with some extensions.

For the mass-spring system shown in Fig. 1 that is continuously excited with the external force $F(t)$, the equation of motion of the system can be written as

$$m\frac{d^2x}{dt^2} + b\frac{dx}{dt} + kx = -F\sum_n \delta(t-t_n)\operatorname{sgn}(x(t_{n-1}))\,, \tag{1}$$

where m is the mass of the movable plate, b is the damping factor, k is the spring factor, F is the amplitude of impulses, which affect the system at the moments $t_n = nT_s$, $\delta(t)$ is the Dirac delta function and $\operatorname{sgn}(x)$ is the sign-function

$$\operatorname{sgn}(x) = \begin{cases} 1, & \text{if } x \geq 0, \\ -1, & \text{if } x < 0. \end{cases}$$

The resonator is assumed to be underdamped, i.e. $0 < b < 4km$.

Introducing the velocity $v(t) = dx/dt$ and a linear change of variable $y = -\frac{\beta}{\sqrt{1-\beta^2}}x - \frac{1}{\omega_0\sqrt{1-\beta^2}}v$ we transform (1) into the convenient symmetrical form

$$\frac{d}{dt}\begin{pmatrix} x(t) \\ y(t) \end{pmatrix} = \begin{pmatrix} -\beta & -\sqrt{1-\beta^2} \\ \sqrt{1-\beta^2} & -\beta \end{pmatrix}\begin{pmatrix} x(t) \\ y(t) \end{pmatrix} \tag{2}$$

$$y(nT_s+) - y(nT_s-) = Y\operatorname{sgn}(x(nT_s - T_s))\,,$$

where $\beta = b/(2\sqrt{km})$ is the dimensionless damping factor, $\omega_0 = \sqrt{k/m}$ is the natural frequency of the resonator and $Y = \frac{F}{\omega_0 m\sqrt{1-\beta^2}}$ is the normalized increment.

The 2D iterative map obtained in [Teplinsky & Feely, 2008] from the continuous-time system described by Eq. (2) is the following:

$$\begin{pmatrix} x_{n+1} \\ y_{n+1} \end{pmatrix} = f\begin{pmatrix} x_n \\ y_n \end{pmatrix} \overset{\text{def}}{=} a\mathbf{R}(2\pi r)\begin{pmatrix} x_n \\ y_n \end{pmatrix} + \begin{pmatrix} 0 \\ Y \end{pmatrix}\operatorname{sgn}(x_n)\,, \tag{3}$$

where $x_n = x(nT_s)$ and $y_n = y(nT_s)$ are the values of x and y at the sampling instants $t_n = nT_s$, $r = T_s\dfrac{\omega_0}{2\pi}\sqrt{1-\beta^2}$ is the normalized sample ratio (proportional to the sample ratio $f_0/f_s = T_s\dfrac{\omega_0}{2\pi}$ used in [Dominguez *et al.*, 2005]), $a = \exp(-2\pi\frac{\beta}{\sqrt{1-\beta^2}}) \in (0,1)$ is the contraction factor and $\mathbf{R}(\alpha) = \begin{pmatrix} \cos\alpha & -\sin\alpha \\ \sin\alpha & \cos\alpha \end{pmatrix}$ is the matrix of the rotation by angle α.

From (3) it follows that if there exists a periodic trajectory for a given value of $Y > 0$, then the same trajectory exists for any other positive value of Y, bur resized appropriately. We may assume, therefore, that $Y = 1$.

It has been observed in [Dominguez *et al.*, 2005] that the normalized digital frequency as a function of the sampling ratio is similar to the devil's staircase [Hilborn, 2000]. Its presence is connected with the mode-locking (or frequency-locking), that is common whenever two or more processes each with its own frequency interact nonlinearly. The oscillations are frequency-locked if one frequency is a rational number times the other frequency. Thus, it is natural to consider the rotation number for Eq. (3): if it is a rational number, then the resulting oscillations are periodic.

The rotation number is defined as follows: for a point $(x, y) \neq (0, 0)$, the polar angle $\alpha = \angle(x, y)$ is a real number defined up to an integer multiple of 2π. To each point of a trajectory (x_n, y_n), the angle α_n can be set up in correspondence, such that $\alpha_1 \in [0, 2\pi)$ and $\alpha_{n+1} \in [\alpha_n, \alpha_n + 2\pi)$ for every $n \geq 1$. The rotation number for this trajectory is defined as

$$\rho = \lim_{n\to\infty} \frac{\alpha_n}{2\pi n} \in [0, 1]\,. \tag{4}$$

If the limit in (4) exists, it is invariant with respect to shifts in the index n, so the rotation number is a function of the trajectory as a whole. It shows how many times the trajectory winds around the origin in a single step.

Figure 2 shows the plot of rotation number ρ as a function of normalized sampling ratio r [a]. The values have been obtained by calculating the ratio (4) for at least $n = 5000$ trajectory points. This plot is similar to the one presented in [Dominguez *et al.*, 2005].

There is one case when the limit in (4) is guaranteed to exists, and that is when the trajectory approaches a stable limit cycle, i.e. a periodic trajectory that attracts nearby trajectories. If a trajectory approaches a limit cycle of length N, then its rotation number ρ is a rational number of the form M/N. The only type of behaviour we have observed in our simulations is associated with rational rotation numbers, i.e. any observed trajectory

---

[a] All graphs and parameter planes presented in this paper calculated with zero initial conditions, except plots with basins of attraction.

eventually approaches some limit cycle. Note that the oscillation frequency in this case is given by ρ/T_s.

Figure 3a shows the 8-cycle of the map (3) with $\rho = 3/8$. To demonstrate how this picture relates to the original continuous-time system, we depict in Fig. 3b the phase portrait obtained from the solution of Eqs. (2) at the same values of β and r. For the continuous-time system (2), the trajectory in phase space is a closed curve that corresponds to periodic motion with eight kicks over three rotations in phase space. The points of the stroboscopic map (i.e. the points extracted from the trajectory in each interval of time T_s) are shown by circles in Fig. 3b.

Note that Eq. (1) is invariant under the change of variable $x \to -x$, so limit cycles are symmetrical with respect to the origin (for even N) or co-exist with symmetrical copies (for odd N).

Figure 4 shows the (β, r) parameter plane for the map (3). Each coloured region corresponds to the domain of existence of a particular limit cycle with $3 < N < 16$. For the widest tongues the values of the rotation numbers are given in the figure.

The whole picture looks similar to what we have for a first-order sigma-delta modulator (see [Feely & Chua, 1991], Fig. 10), but in this case the tongues overlap and the system demonstrates multistability. This means that for certain values of β and r there are coexisting limit cycles of different orders with different values of rotation number ρ. The initial values x_0 and y_0 dictate which one of them will eventually be approached by a particular trajectory. Figure 5 illustrates the case when three tongues overlap, and four limit cycles (a pair of 5-cycles with $\rho = 2/5$, the 18-cycle with $\rho = 7/18$ and the 8-cycle with $\rho = 3/8$) coexist. It is worth noting that the basins of attraction for the 8-cycle and the 18-cycle both touch the origin. This means that if any deviation from the nominal initial state at the origin is present, it will be impossible to predict which regime will finally be exhibited by the system.

To conclude this section let us discuss the correspondence between the description provided by the differential equation (2) and by the map (3). It is convenient to use the dimensionless parameter $T = \omega_0 T_s$ ($\omega_0 T_s \approx 2\pi r$ for small values of β) to illustrate results. Figure 6 shows the tongues in the parameter plane calculated by using the method of Poincaré mapping [Hilborn, 2000]. This figure also shows several examples of the limit cycles one can observe in this system [b]. The structure of the tongues is very similar to the one presented in Fig. 4 for the iterative map. On the parameter plane we show the tongues of the N-cycles for $N \leq 16$. The largest tongues are the "main" tongue that corresponds to the 4-cycle with $\rho = 1/4$ and the tongues that correspond to the limit cycles with small values of $N < 10$.

Note that nominally each tongue tends to a certain point T_N on the T-axis. One can understand which tongue is which by estimating a value of T_N. Then, the value of the rotation number ρ for each tongue is defined as $\rho = T_N/(2\pi)$. The smaller the length of a limit cycle, the more precisely one can calculate numerically the bound of its tongue near the vertical axis at $\beta \to 0$.

The whole picture agrees with the results we have presented in this section for the map (3) and we can conclude that the map provides an adequate description of the system.

3. Nonlinear Resonator

Now we incorporate nonlinearity in the mechanical part of the MEMS oscillator in Fig. 1 into our model. We consider that the spring in the MEMS resonator is a nonlinear element and use the well-known formula for its recovery force $F_s(x) = kx + \alpha x^3$. This form of $F_s(x)$ includes the term that describes the higher-order stiffening effect and has been used in [Zhang *et al.*, 2002; Zhang & Meng, 2005; Zhang & Meng, 2007; Mestrom *et al.*, 2008] to model different types of MEMS oscillators. Now Eq. (1) can be generalised by adding a cubic nonlinear term and rewritten in the following form

$$m\frac{d^2x}{dt^2} + b\frac{dx}{dt} + kx + \alpha x^3 = -F\sum_n \delta(t - t_n)\mathrm{sgn}(x(t_{n-1}))\,, \tag{5}$$

where α is the cubic nonlinear constant. Depending on the sign of the constant α, we distinguish two cases: "spring softening" for $\alpha < 0$ and "spring hardening" for $\alpha > 0$. (The first case corresponds to a mechanical oscillator with a spring whose restoring force increases with increasing displacement, while the second case describes a spring whose restoring force decreases with increasing displacement.)

In [Palaniapan & Khine, 2008] the authors note that mechanical nonlinearities usually result in a positive value of α (spring hardening), whereas electrical nonlinearities

---

[b] The correspondence between a limit cycle of Eq. (2) and a one of map (3) is illustrated by the example of Fig. 3.

tend to give rise to negative α (spring softening). However, depending on the resonator architecture, mechanical nonlinearities could also give rise to spring softening, so it is reasonable to examine both types of nonlinearity.

We note that Eq. (5) is similar to the periodically kicked nonlinear dissipative oscillator studied in [Kuznetsov *et al.*, 2001]. The equation studied in the latter paper has the same left side, but the sign of the kicks is constant.

It is convenient to use a dimensionless time in (6): $\tau = \omega_0 t$, where $\omega_0 = \sqrt{k/m}$. Thus, the oscillator is now described by

$$\frac{d^2x}{d\tau^2} + \gamma\frac{dx}{d\tau} + x + \varepsilon x^3 = -F_0 \sum_n \delta(\tau - nT)\,\mathrm{sgn}(x(\tau_{n-1}))\,, \tag{6}$$

where

$$\begin{aligned} \gamma &= \frac{b}{\sqrt{km}}\,, & \varepsilon &= \frac{\alpha}{m\omega_0^2}\,, \\ F_0 &= \frac{F}{\omega_0 m}\,, & T &= \omega_0 T_s\,. \end{aligned} \tag{7}$$

In Eq. (6) x is the position of the oscillator, γ is the dimensionless parameter of dissipation, ε is the cubic nonlinear constant, F_0 is the dimensionless amplitude of the kick and T is the interval between them. Note that the parameter ε may be positive or negative. From definition (7) one can set the correspondence between the parameters in (6) and the parameters used in Sec. 2.

$$\begin{aligned} &\gamma = 2\beta\,, \qquad T = \frac{2\pi}{\sqrt{1-\beta^2}}r\,, \\ &F_0 = Y\sqrt{1-\beta^2}\,. \end{aligned} \tag{8}$$

For small values of β, $T \approx 2\pi r$ and $F_0 \approx Y$. In (6) the parameter T is the one that is similar to the normalized sampling ratio r (it is proportional to the sampling ratio f_0/f_s from [Dominguez *et al.*, 2005], $T = 2\pi f_0/f_s$).

We can obtain an iterative map from the original equation (6) using the method of slow amplitudes [Nayfeh & Mook, 1995]. Kuznetsov *et al.* [2001] also apply this method to the oscillator under investigation in that work. The idea is to find the approximate solution of (6) between kicks. We represent the displacement x in the following form

$$x(\tau) = \frac{a(\tau)}{2}e^{i\tau} + \frac{a(\tau)^*}{2}e^{-i\tau}\,, \tag{9}$$

where $a(\tau)$ is the slowly varying amplitude and $a(\tau)^*$ is the complex conjugate of $a(\tau)$. Since we have introduced the complex variable $a(\tau)$ instead of the real $x(\tau)$, we can use the additional condition:

$$\frac{\dot{a}(\tau)}{2}e^{i\tau} + \frac{\dot{a}(t)^*}{2}e^{-i\tau} = 0\,. \tag{10}$$

Substituting (9) into (6) and taking into account condition (10), after averaging over time we obtain the truncated equation

$$\dot{a} = -\frac{\gamma}{2}a + \frac{3}{8}\,i\,\varepsilon|a|^2 a\,. \tag{11}$$

Now we can represent the complex amplitude $a(t) = R(t)e^{i\varphi}$ using real amplitude R and phase φ and rewrite Eq. (11) in real variables

$$\begin{aligned} \dot{R} &= -\frac{\gamma}{2}R\,, \\ \dot{\varphi} &= \frac{3}{8}\varepsilon R^2\,. \end{aligned} \tag{12}$$

Equations (12) allow us to find the amplitude and the phase as functions of time just after the n-th kick. We can also use them to define the position x and the velocity v of the oscillator via the amplitude R and the phase φ

$$\begin{aligned} x(\tau) &= R(\tau)\cos(\tau + \varphi(\tau))\,, \\ v(\tau) &= -R(\tau)\sin(\tau + \varphi(\tau))\,. \end{aligned} \tag{13}$$

The solution of (12) is

$$\begin{aligned} R &= R_n e^{-\gamma\tau/2}\,, \\ \varphi &= \frac{3}{8}\varepsilon R_n^2\frac{1-e^{-\gamma\tau}}{\gamma} + \varphi_n\,. \end{aligned} \tag{14}$$

Substituting the latter equations into (13), we find the position and the velocity of the oscillator after the n-th kick as functions of time. Owing to the nature of the external force, immediately after each kick the position does not change, whereas the the velocity changes its value by $+F_0$ or $-F_0$ depending on the previous position of the resonator:

$$\begin{aligned} x_{n+1} &= R_n e^{-\gamma T/2}\cos\left(T + \frac{3}{8}\varepsilon|R_n|^2\frac{1-e^{-\gamma T}}{\gamma} + \varphi_n\right)\,, \\ v_{n+1} &= -R_n e^{-\gamma T/2}\sin\left(T + \frac{3}{8}\varepsilon|R_n|^2\frac{1-e^{-\gamma T}}{\gamma} + \varphi_n\right) - F_0\,\mathrm{sgn}(x_n)\,. \end{aligned} \tag{15}$$

It is conventional to rewrite Eqs. (15) in complex form

$$z_{n+1} = B\,z_n e^{(\pm i|z_n|^2 + iT)} - A\,\mathrm{sgn}(\mathrm{Im}(z_n))\,, \tag{16}$$

where

$$\begin{aligned} z &= (v + ix)\sqrt{\frac{3\,|\varepsilon|}{8}\frac{1-e^{-\gamma T}}{\gamma}}\,, \\ A &= F_0\sqrt{\frac{3\,|\varepsilon|}{8}\frac{1-e^{-\gamma T}}{\gamma}}\,, \qquad B = e^{-\gamma T/2}\,. \end{aligned} \tag{17}$$

The sign before the term $i|z_n|^2$ in the exponent in (16) is defined by the sign of the constant ε.

Note that the method of slow amplitudes allows us to find only the approximate solution of Eq. (6). Nominally, this method is valid for small values of the dissipation and nonlinear parameters $\gamma, \varepsilon \ll 1$ where the system is close to the harmonic conservative oscillator. The plane of parameters (γ, T) calculated for Eq. (6) is presented in Fig. 7. Comparing it with Fig. 8b calculated at the same value of ε for the map (16), one can see that two plots look quite similar, i.e. the map captures the principal features of the system dynamics over the full range of values of γ.

The pulse driven nonlinear oscillator studied in [Kuznetsov *et al.*, 2001] can be reduced to the Ikeda map [Ikeda *et al.*, 1997]. In our case, we obtain the map (16) which is similar to the Ikeda map with the difference that the kick sign is given by the sign of the oscillator coordinate. Conventionally, the Ikeda equation is studied in terms of parameters given by relations (7). Here we study the map written in the form (16), but present results using the dissipation parameter γ and the sampling ratio T in order to compare the results with those obtained in [Teplinsky & Feely, 2008] and summarised in Sec. 2.

From (7) it follows that if an attractor exists at the values of the impulse amplitude F_{0_1} and the nonlinear constant ε_1, the same exists at F_{0_2} and ε_2 if $F_{0_1}\sqrt{\varepsilon_1} = F_{0_2}\sqrt{\varepsilon_2}$. We choose $F_0 = 1$ as in Sec. 2 and several values of ε to monitor changes in the dynamics of the system.

Figure 8 illustrates the transformation of tongues in the parameter plane for map (16) with increasing ε in case of the spring hardening effect (i.e. $\varepsilon > 0$). In the limit $\varepsilon \to 0$ we come to the linear case (but note that from definitions (17) it follows that it is impossible to consider precisely $\varepsilon = 0$). Figure 8a is calculated at the very small value of nonlinear constant $\varepsilon = 10^{-4}$ to show the correspondence with Fig. 4. Note that in general the smaller the dissipation, the more iterations a trajectory needs to reach a steady state.

As is seen from the figure, even weak nonlinearity leads to distortion of tongues; this effect being especially noticeable for small values of the dissipation parameter γ. This is worth noting since a typical MEMS resonator has a small damping factor. For instance, the simulations in [Dominguez *et al.*, 2005] have been carried out at $\beta = \gamma/2 =$

$8.24 \cdot 10^{-3}$.

The blank areas in the parameter plane correspond not only to longer period limit cycles but also to more complex trajectories, particulary when the nonlinear parameter is large. To illustrate this we plot phase portraits for different values of ε at γ and T taken from the blank region of the planes from Fig. 8. Figure 9a shows the 29-cycle eventually reached by a trajectory started from the origin after 5000 iterations in the weakly nonlinear system ($\varepsilon = 0.0001$). Figure 9b illustrates the much more complex phase portrait obtained for $\varepsilon = 0.001$ after at least 100000 initial iterations.

As in the linear case, tongues corresponding to limit cycles of different length may overlap. One important conclusion shown by the example of Fig. 5 is that the basins of different attractors may touch the origin or lie close to it (see Sec. 2). First, we present an example that is similar to the linear case shown in Fig. 5. Figure 8d shows the structure of the basins of attraction for the 5-, 8- and 18-cycles calculated from map (16) at $\varepsilon = 0.001$. The values of the parameters γ and T for this plot correspond to those parts of the tongues which are not affected by the distortion. Moreover, after transforming the variable z to the variables x and y used in Sec. 2 and resizing the figure appropriately according to (17), we will obtain the same plot as shown in Fig. 5.

In the region of small values of the dissipation parameter γ where we observe the distortion of tongues caused by the nonlinearity, tongues overlap forming quite complicated basins of attraction. For instance, Fig. 10a shows the basins of attraction of several limit cycles which appear due to the deformation of tongues ($\varepsilon = 0.001$). The latter example demonstrates the coexistence of the 3-, 8-, 14-, 32-cycles with the rotation numbers $\rho = 1/3$, $3/8$, $5/14$ and $11/32$ respectively. A zoom of the central region is shown in Fig. 10b: the region around the origin is formed by the basins of the 3- and 32-cycles. Figure 11 illustrates the basins of attraction in the case $\varepsilon = 0.005$.

To calculate the rotation number for map (16), we use the formula (4), where we consider α_n to be the sequence of arguments of the complex variable z_n. The rotation number ρ as a function of the parameter T is shown in Fig. 12 for $\varepsilon = 0.001$. The plot (a) is calculated at the constant value of dissipation $\gamma = 0.03$ and combined with the bifurcation diagram $x_n(T)$ for additional visualisation. For the widest steps of the graph, the values of the rotation numbers are given. The plot (b) shows the transformation of the graphs of $\rho(T)$ with increasing the dissipation parameter γ.

As the nonlinear parameter ε is increased, tongues become strongly deformed, that effect being especially visible on the plots of $\rho(T)$ at a constant γ (Fig. 13). It is possible to observe the same limit cycle over a wide range of values of T. Figure 13a shows the example of $\rho(T)$ and a bifurcation diagram $x_n(T)$ at $\gamma = 0.03$, where the 8-limit cycle with $\rho = 3/8$ is observed over the range $1 < T < 2$.

Note that spring hardening leads to distortion of tongues with rotation numbers $\rho \geq 1/4$ in the region of small values of dissipation. When the dissipation parameter is large enough, a plot of $\rho(T)$ is very similar to the one we have in the linear case (for instance, compare the graph in Fig. 12 at $\varepsilon = 0.001$ and $\gamma = 0.1$ with Fig. 2). When dissipation is small, the structure of the graphs changes and one can observe only limit cycles with $\rho \geq 1/4$. This is easy to see from with the planes of parameters shown in Fig. 8 : when we calculate the rotation number as a function of the sampling ratio, we "move" along the T–axis at a constant value of γ on the (γ, T) plane, and steps of the $\rho(T)$ graph correspond to crossing particular tongues. At small values of γ we can "intersect" only the deformed tongues, which means that the whole graph will lie above the "nominal" graph for the linear case.

Now let us turn to results for the spring softening effect, i.e. for $\varepsilon < 0$. A series of pictures showing parameter planes for different values of the nonlinear constant ε is presented in Fig. 14. As in the case of positive ε, the nonlinearity causes distortion of the tongues. In contrast to the previously considered case of the "spring hardening" effect, the distortion concerns the tongues with the rotation numbers $\rho \leq 1/4$.

Tongues may overlap like in all previous cases. First of all, Fig. 14d illustrates the basins of attraction similar to the example shown in Fig. 8d. The plot in Fig. 14d is calculated for those tongues that are not deformed by the presence of nonlinearity. Fig. 15a shows the basins of attraction that appear due to the deformation of tongues in the region of small values of the dissipation parameter. A zoom of the central region near the origin is shown in Fig. 15b. Fig. 16 shows the basins of attraction in the region of tongue deformation for a strongly nonlinear resonator ($\varepsilon = -0.005$). Note that the basins in the region of the tongue deformation typically have the same structure near the origin, i.e. four bands spiraling away from the origin.

Figure 17 shows how graphs of the rotation number ρ versus the parameter T change with decreasing dissipation: plot (a) is calculated at $\varepsilon = -0.001$ and plot (b) is calculated at $\varepsilon = -0.005$. The lower the dissipation, the wider the steps of the graph become.

The spring softening effect also leads to deformation of tongues, but this time it concerns the tongues with $\rho \leq 1/4$. The essential difference from spring hardening is that the $\rho(T)$ plots for small dissipation are situated in the lower part of the (γ, T) plane and its steps are associated with the deformed tongues.

4. Conclusion

In this paper, we have presented the results of a study of the MEMS oscillator from [Dominguez *et al.*, 2005]. The problem has been generalised to include mechanical nonlinearity in the resonator. The resonator has been described as a damped linear or nonlinear oscillator kicked at a fixed period of time with the sign of each kick defined by the sign of the position of the oscillator. Due to the constant frequency of the kicks, the differential equations can be reduced to iterative maps.

We began by summarising the results of [Teplinsky & Feely, 2008] concerning the linear resonator, and also presented some extensions of that work. We then proceeded to the system that was our primary focus in this paper: the resonator with mechanical nonlinearity described by the Duffing equation. For the linear system, the study of limit cycles in state space and their rotation numbers has been reviewed. It has been shown that the oscillator output is sensitive to initial conditions, i.e. depending on the initial coordinate and velocity the oscillator demonstrates different regimes. Moreover, the basins of attraction plotted on the plane position–velocity may lie close to the origin. This means that in a practical system allowing for the presence of noise one cannot predict to which limit cycle a trajectory starting nominally at the origin will converge. We also have presented the plane of parameters calculated for the original continuous-time system and have shown the correspondence between the description of the system in terms of the differential equation and the iterative map.

For the nonlinear resonator we have shown that nonlinearity causes additional effects besides those observed in the linear system. First of all, regions of existence of particular limit cycles (tongues) on the plane of controlling parameters become deformed even if the nonlinearity is small. Due to the distortion of the tongues, for the nonlinear system at very small values of the dissipation parameter γ the output are limit cycles with a limited set of values of rotation numbers: $\rho \geq 1/4$ for positive values of the nonlinear constant ε and $\rho \leq 1/4$ for negative ε. The basins of attraction typically have a structure of a spiral; the area around the origin are formed by basins of two and more limit cycles. In contrast to the linear case where low-period limit cycles are predominant, in the nonlinear system we have also observed more complex steady-state behaviour.

Acknowledgments

The authors would like to thank Dr. A. Teplinsky for useful discussions. The work was supported in part by Science Foundation Ireland.

References

Bao, M. & Wang, W. [1996] "Future of microelectromechanical systems (MEMS)", *Sensors and Actuators A* , **56**, 135-141.

Dominguez, M., Pons, J., Ricart, J. & Bermejo, A. [2004] "A sigma-delta digital oscillator for MEMS", *Sensors, 2003. Proceedings of IEEE*, **2**, 834–838.

Dominguez, M., Pons-Nin, J., Ricart, J., Bermejo, A., Costa, E.F. & Morata, M. "Analysis of the $\Sigma - \Delta$ Pulsed Didgital Oscillator for MEMS", *IEEE Trans. on Circuits and System I*, **52**(11), 2286–2297.

Dominguez, M., Pons, J. & Ricart, J. [2007] "Application of Pulsed Digital Oscillator in 'reverse mode' to eliminate undesired vibrations in high-Q MEMS resonator", *Proc. IEEE. Int. Symp. Circuits and Systems*, New Orleans, May 2007, 925-928.

Feely, O. & Chua, L.O. [1991] "The effect of integrator leak in $\Sigma\Delta$ modulation", *IEEE Trans. Circuits and Systems*, **38**, 1293–1305.

Feely, O. [2007] "Nonlinear dynamics of discrete-time circuits: a survey", *Int J. Circuit Theory and Applications*, **35**, 515–531.

Gui, C., Legtenberg, R., Tilmans, H.A.C., Fluitman, J.H.I. & Elwenspoek, M. [1998] "Nonlinearity and hysteresis of resonant strain gauges" *Jouranl of microelectromechanical systems*, **7**(1), 122–127.

Hilborn R.C. *Chaos and Nonlinear Dynamics: an Introduction for Scientists and Engineers.* (Oxford University Press, Oxford).

Ikeda, K., Daido, H. & Akimoto, O. [1980] "Optical Turbulence: Chaotic Behaviour of transmitted light from a ring cavity", *Phys. Rev. Lett*, **45**(9), 709-712.

Kuznetsov, A.P., Turukina, L.V. & Mosekilde, E. [2001] "Dynamical systems of different classes as models of the kicked nonlinear oscillator", *Int. Journal of Bifurcation and Chaos*, **11**(4), 1065–1077.

Kuznetsov A.P. & Tyuryukina L.V. [2003] "Forced Synchronization in a System with Unstable Cycle", Tech. Phys. Lett., **29**(4), 332-333.

Kuznetsov A.P., Stankevich N. V. & Tyuryukina L. V. [2006] "Features of Pulsed Synchronization of an Autooscillatory System with a Three-Dimensional Phase Space", Tech. Phys. Lett., **32**(4), 343-34.

Langdon, R.M. [1985] "Resonant Sensors — a Review", *J. Phys. E: Sci. Instrum.* **18**(2), 103–115.

Mestrom, R.M.C., Fey, R.H.B., van Beek, J.T.M., Phan, K.L. & Nijmeijer, H. [2008] "Modelling the dynamics of a MEMS resonator: simulations and experiments", *Sensors and Actuators*, **A142**, 306–315.

Mudde, R.F. & Jansz, S.G. "Influence of damping on the delta-kicked harmonic oscillator with Heaviside kick", *Physica*, **D179**, 1–17.

Nayfeh, A.H. & Mook, D.T. [1995] *Nonlinear Oscillations* (John Wiley & Sons, Inc., New-York).

Norsworthy, R.S., Schreier, R. & Temes, G.C. (eds.) [1997] *Delta-Sigma Data Converters. Theory, Design, and Simulatios* (IEEE Press, New York).

Palaniapan, M. & Khine, L. [2008] "Nonlinear behavior of SOI free-free micromechanical beam resonator", *Sensors and Actuators A*, **142**, 203–210.

Parsons, P. [1993] "Resonant Sensors", *IEE Colloquium on Measurement Using Resonant Sensing.*

Scott, A.J., Holmesa, C.A. & Milburn, G.J. [1997] "Hamiltonian mappings and circle packing phase spaces", *Physica*, **D155**, 34–50.

Teplinsky, A. & Feely, O. [2008] "Limit Cycles in a MEMS Oscillator", *IEEE Transactions on Circuits and Systems II: Express Briefs* (to appear).

Zhang, W., Baskaran, R. & Turner, K.L. [2002] "Effect of cubic nonlinearity on auto-parametrically amplified resonant MEMS mass sensor", *Sensors and Actuators A*, **102**, 139–150.

Zhang, W. & Meng, G. [2005] "Nonlinear dynamical system of micro-cantilever under combined parametric and forcing excitations in MEMS", *Sensors and Actuators A*, **119**, 291–299.

Zhang, W. & Meng, G. [2007] "Nonlinear Dynamic Analysis of Electrostatically Actuated Resonant MEMS Sensors Under Parametric Excitation", *IEEE Sensors Journal*, **7**, 370–379.

Fig. 1. The MEMS oscillator described in [Dominguez *et al*, 2005].

Fig. 2. Rotation number ρ as a function of the normalized sample ration r, $\beta = 0.05$; (b) is a zoom of (a).

Fig. 3. The limit cycle of the map (3) with $\rho = 3/8$ at the parameter values $\beta = 0.05$, $r = 0.39$ (a); the limit cycle of the continuous-time system (2) at the same values of the parameters (b). The points of the stroboscopic map are shown by circles in the latter plot.

Fig. 4. Tongues in the parameter plane for map (3). The regions correspond to limit cycles with rotation numbers $\rho = M/N$, where $3 \leq N \leq 16$.

Fig. 5. Coexisting limit cycles and their basins of attraction for the parameter values $\beta = 0.05$, $r = 0.042$. Trajectories starting from the inner light gray region approach the 8-cycle shown by square marks with $\rho = 3/8$; those starting from the white region approach the 18-cycle shown by circles with $\rho = 7/18$; trajectories starting from the outer dark gray region approach one of the symmetric pair of 5-cycles with $\rho = 2/5$, one of which is shown by circles and the other by squares.

Fig. 6. Tongues in the parameter plane $(\beta\,, \omega_0 T_s)$ calculated for Eq. (2) and the phase portraits at the following values of parameters: $\beta = 0.1$ and $\omega_0 T_s =$ (1) 3.1, (2) 2.6, (3) 2.2, (4) 1.5, (5) 1.2, (6) 1.0, (7) 0.9, (8) 0.7.

Fig. 7. Tongues in the parameter plane $(\gamma\,, T)$ calculated for Eq. (6), $\varepsilon = 0.001$.

Fig. 8. Transformation of tongues of the map (16) with $3 \leq N \leq 16$ on the the parameter plane: $\varepsilon = 0.0001$ (nearly linear case) (a), $\varepsilon = 0.001$ (b), $\varepsilon = 0.005$ (c). The case $\varepsilon \to 0$ corresponds to the plane depicted in Fig. 4. Coexisting limit cycles and their basins of attraction (d) for the parameter values $\varepsilon = 0.001$, $\gamma = 0.1$, $T = 2.6325$. Depending on the starting conditions, trajectories approach either the 8-cycle (squares) with $\rho = 3/8$, the 18-cycle (circles) with $\rho = 7/18$ or one of the symmetric pair of 5-cycles (one of which is shown by squares and connected) with $\rho = 2/5$.

Fig. 9. Steady-state trajectories of the map (16) calculated at $\varepsilon = 0.0001$ (a) and $\varepsilon = 0.001$ (b); $\gamma = 0.06$, $T = 0.4$ for both plots.

Fig. 10. Basins of attraction of coexisting limit cycles for the parameter values $\varepsilon = 0.001$, $\gamma = 0.02$, $T = 1.5$. Trajectories starting in different regions approach either one of the symmetric pair of 3-cycles with $\rho = 1/3$, the 8-cycle with $\rho = 3/8$, the 14-cycle with $\rho = 5/14$ or the 32-cycle with $\rho = 11/32$. Plot (b) is a fragment of (a).

Fig. 11. Basins of attraction of coexisting limit cycles for the parameter values $\varepsilon = 0.005$, $\gamma = 0.04$, $T = 1.45$. Trajectories starting in different regions approach either one of the

symmetric pair of 3-cycle with $\rho = 1/3$, the 8-cycle with $\rho = 3/8$, the 14-cycle with $\rho = 5/14$ or the 20-cycle with $\rho = 7/20$.

Fig. 12. Rotation number ρ as a function of the parameter T and bifurcation diagram (a) for the parameter values $\varepsilon = 0.001$, $\gamma = 0.03$. Plots of $\rho(T)$ at different values of the dissipation parameter γ (b).

Fig. 13. Rotation number ρ as a function of the parameter T and bifurcation diagram (a) for the parameter values $\varepsilon = 0.005$, $\gamma = 0.03$. Plots of $\rho(T)$ at different values of the dissipation parameter γ (b).

Fig. 14. Transformation of tongues of the map (16) with $3 \leq N \leq 16$ on the the parameter planes: $\varepsilon = -0.0001$ (nearly linear case) (a) , $\varepsilon = -0.001$ (b), $\varepsilon = -0.005$ (c). The case $\varepsilon \to 0$ corresponds to the plane depicted in Fig. 4. Coexisting limit cycles and their basins of attraction (d) for the parameter values $\varepsilon = -0.001$, $\gamma = 0.073$, $T = 2.78$. Depending on the starting conditions, trajectories approach either the 10-cycle (circles) with $\rho = 3/10$, the 12-cycle (circles) with $\rho = 5/12$ or the 22-cycle (squares) with $\rho = 9/22$.

Fig. 15. Basins of attraction of coexisting limit cycles for the parameter values $\varepsilon = -0.001$, $\gamma = 0.02$, $T = 1.5$. Trajectories starting in different regions approach either one of the symmetric pair of 7-cycles with $\rho = 1/7$, the 6-cycle with $\rho = 1/6$, the 8-cycle with $\rho = 1/8$ or the 20-cycle with $\rho = 3/20$. Plot (b) is a fragment of (a).

Fig. 16. Basins of attraction of coexisting limit cycles for the parameter values $\varepsilon = -0.005$, $\gamma = 0.03$, $T = 1.5$. Trajectories starting in different regions approach either the 8-cycle with $\rho = 1/8$, the 10-cycle with $\rho = 1/10$ or one of the symmetric pair of 11-cycle with $\rho = 1/11$.

Fig. 17. Plots of $\rho(T)$ for the values of dissipation $\gamma = 0.01$, $\gamma = 0.03$, $\gamma = 0.1$. Plot (a) is calculated for $\varepsilon = -0.001$, (b) is for $\varepsilon = -0.005$.

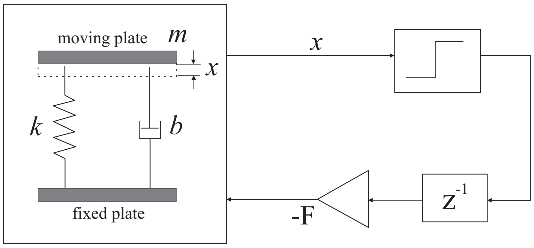

Fig. 1. The MEMS oscillator described in [Dominguez *et al*, 2005].

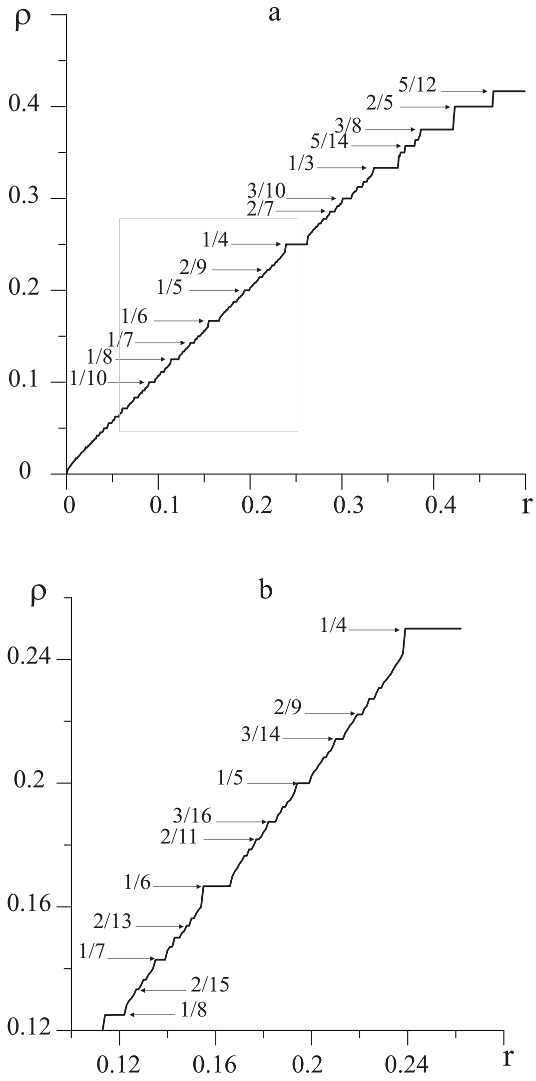

Fig. 2. Rotation number ρ as a function of the normalized sample ration r, $\beta = 0.05$; (b) is a zoom of (a).

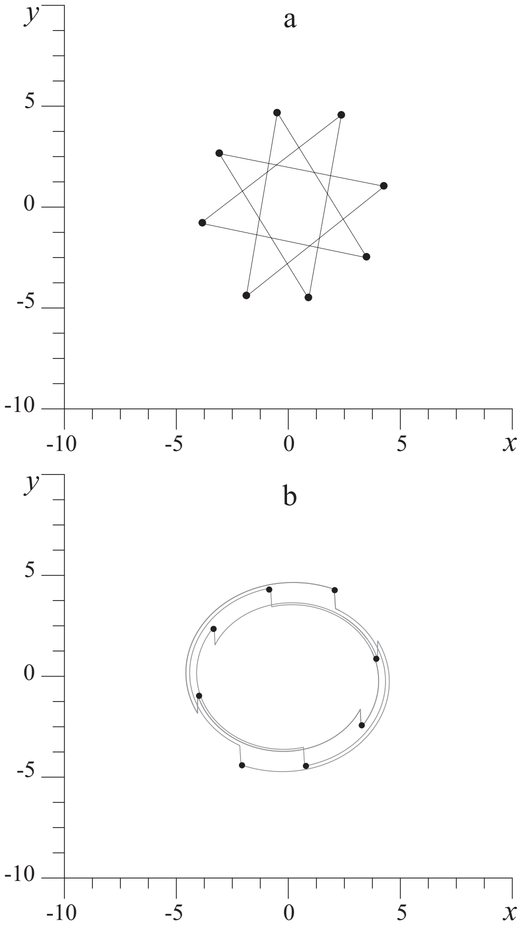

Fig. 3. The limit cycle of the map (3) with $\rho = 3/8$ at the parameter values $\beta = 0.05$, $r = 0.39$ (a); the limit cycle of the continuous-time system (2) at the same values of the parameters (b). The points of the stroboscopic map are shown by circles in the latter plot.

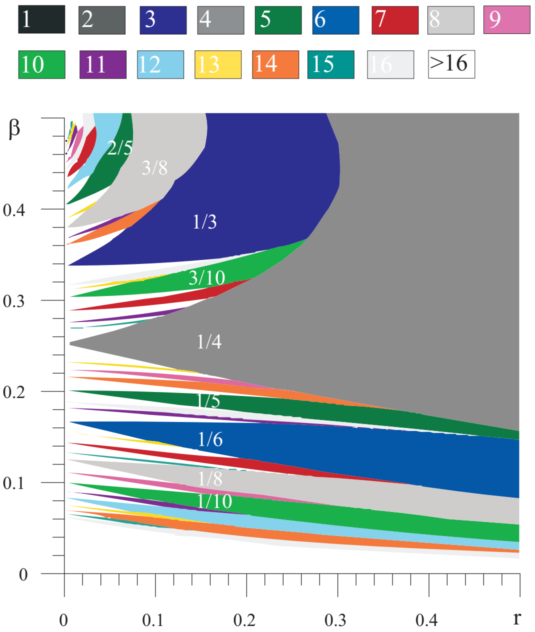

Fig. 4. Tongues in the parameter plane for map (3). The regions correspond to limit cycles with rotation numbers $\rho = M/N$, where $3 \leq N \leq 16$.

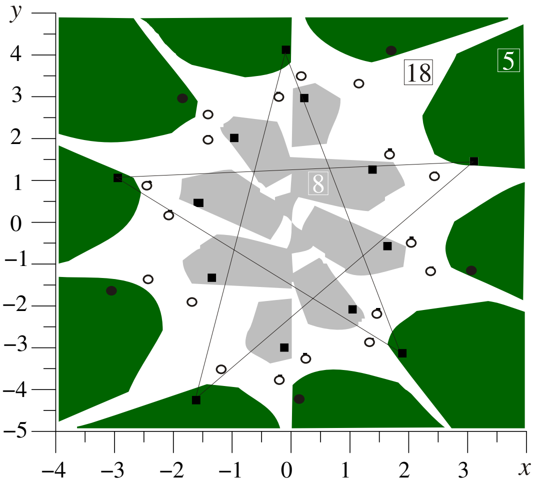

Fig. 5. Coexisting limit cycles and their basins of attraction for the parameter values $\beta = 0.05$, $r = 0.042$. Trajectories starting from the inner light gray region approach the 8-cycle shown by square marks with $\rho = 3/8$; those starting from the white region approach the 18-cycle shown by circles with $\rho = 7/18$; trajectories starting from the outer green region approach one of the symmetric pair of 5-cycles with $\rho = 2/5$, one of which is shown by circles and the other by squares.

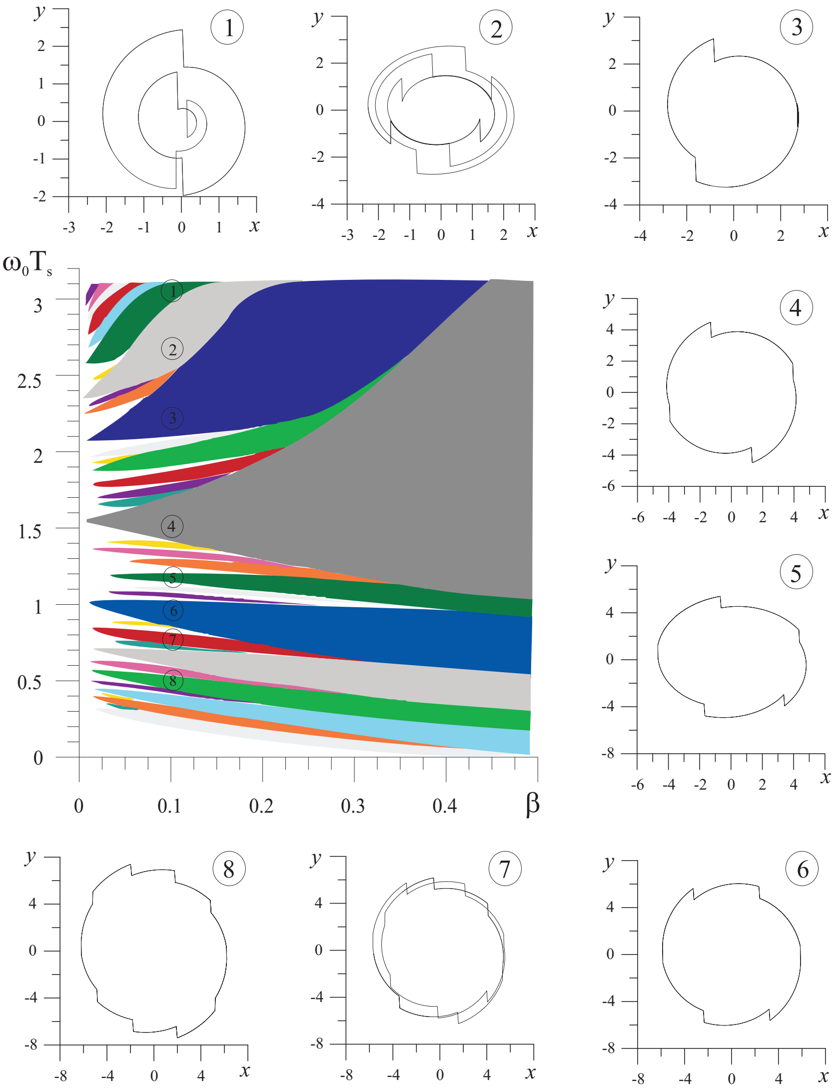

Fig. 6. Tongues in the parameter plane $(\beta\,,\omega_0 T_s)$ calculated for Eq. (2) and the phase portraits at the following values of parameters: $\beta = 0.1$ and $\omega_0 T_s =$ (1) 3.1, (2) 2.6, (3) 2.2, (4) 1.5, (5) 1.2, (6) 1.0, (7) 0.9, (8) 0.7.

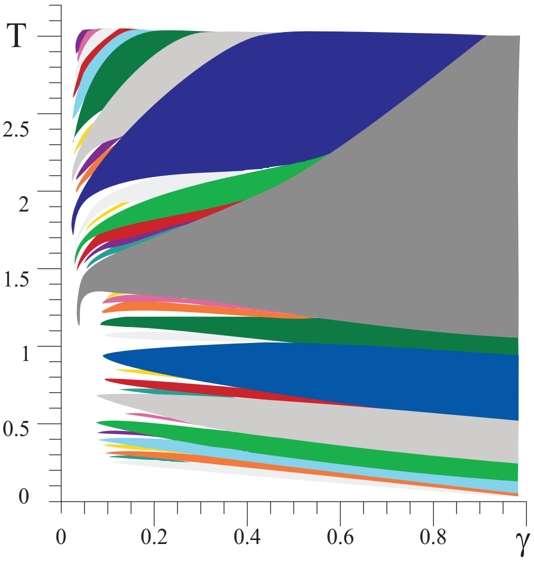

Fig. 7. Tongues in the parameter plane $(\gamma\,, T)$ calculated for Eq. (6), $\varepsilon = 0.001$.

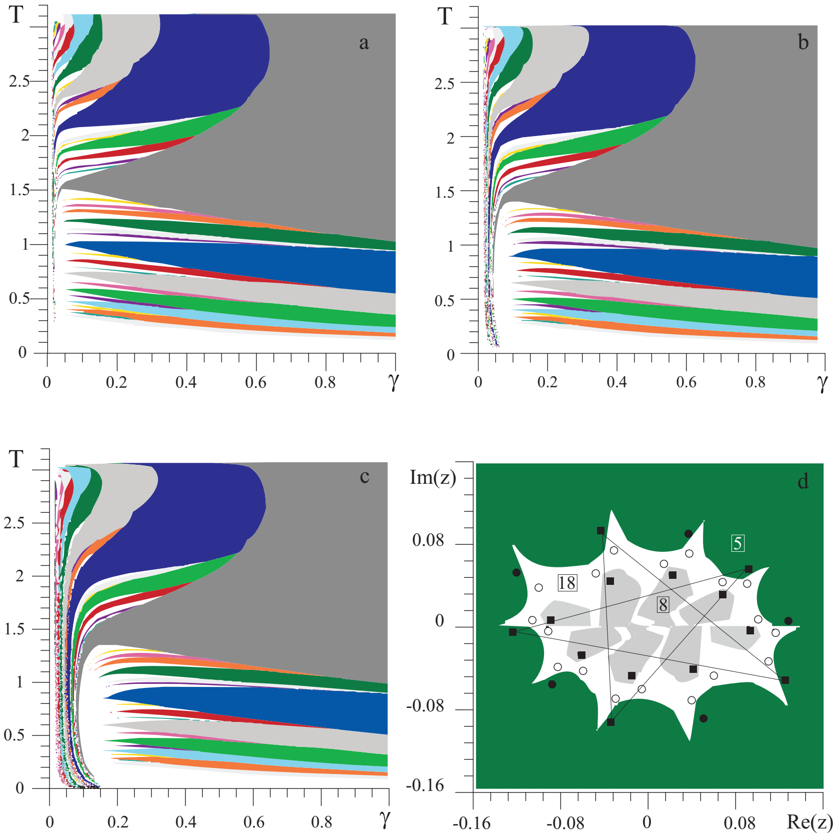

Fig. 8. Transformation of tongues of the map (16) with $3 \le N \le 16$ on the the parameter plane: $\varepsilon = 0.0001$ (nearly linear case) (a), $\varepsilon = 0.001$ (b), $\varepsilon = 0.005$ (c). The case $\varepsilon \to 0$ corresponds to the plane depicted in Fig. 4. Coexisting limit cycles and their basins of attraction (d) for the parameter values $\varepsilon = 0.001$, $\gamma = 0.1$, $T = 2.6325$. Depending on the starting conditions, trajectories approach either the 8-cycle (squares) with $\rho = 3/8$, the 18-cycle (circles) with $\rho = 7/18$ or one of the symmetric pair of 5-cycles (one of which is shown by squares and connected) with $\rho = 2/5$.

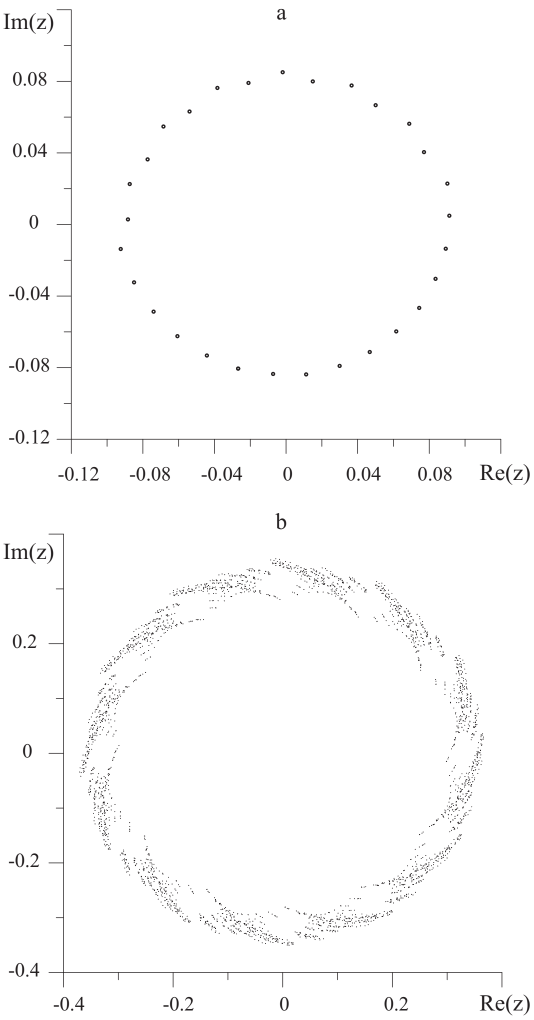

Fig. 9. Steady-state trajectories of the map (16) calculated at $\varepsilon = 0.0001$ (a) and $\varepsilon = 0.001$ (b); $\gamma = 0.06$, $T = 0.4$ for both plots.

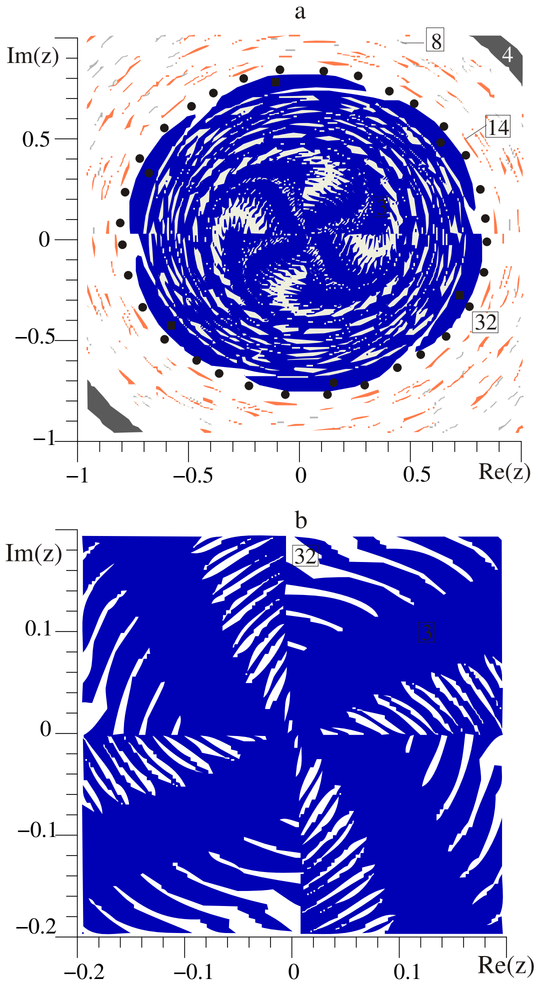

Fig. 10. Basins of attraction of coexisting limit cycles for the parameter values $\varepsilon = 0.001$, $\gamma = 0.02$, $T = 1.5$. Trajectories starting in different regions approach either one of the symmetric pair of 3-cycles with $\rho = 1/3$, the 8-cycle with $\rho = 3/8$, the 14-cycle with $\rho = 5/14$ or the 32-cycle with $\rho = 11/32$. Plot (b) is a fragment of (a).

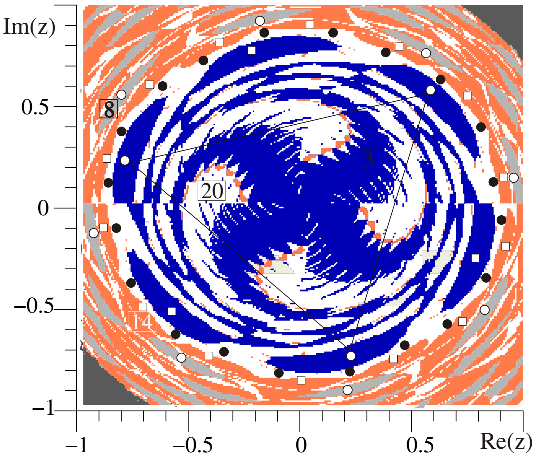

Fig. 11. Basins of attraction of coexisting limit cycles for the parameter values $\varepsilon = 0.005$, $\gamma = 0.04$, $T = 1.45$. Trajectories starting in different regions approach either one of the symmetric pair of 3-cycle with $\rho = 1/3$, the 8-cycle with $\rho = 3/8$, the 14-cycle with $\rho = 5/14$ or the 20-cycle with $\rho = 7/20$.

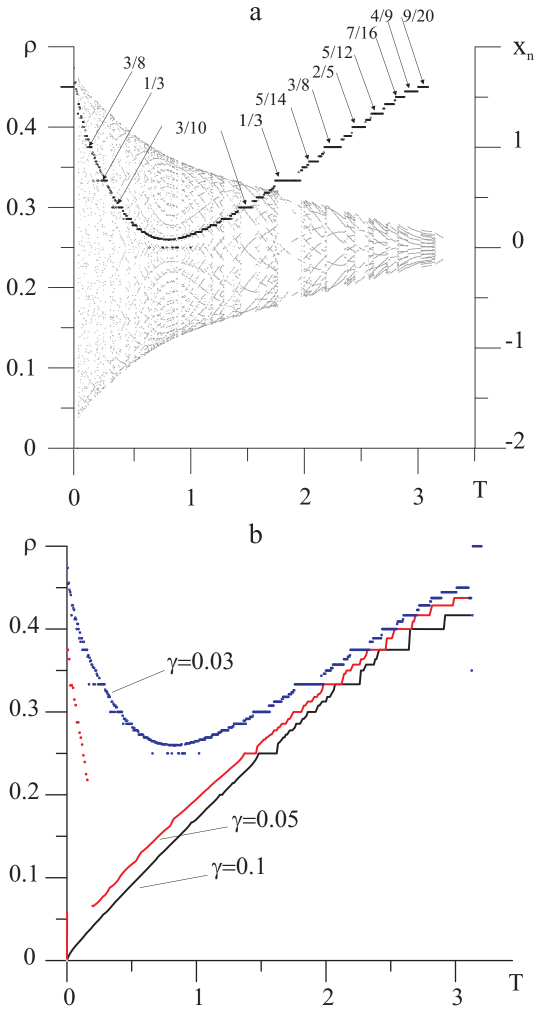

Fig. 12. Rotation number ρ as a function of the parameter T and bifurcation diagram (a) for the parameter values $\varepsilon = 0.001$, $\gamma = 0.03$. Plots of $\rho(T)$ at different values of the dissipation parameter γ (b).

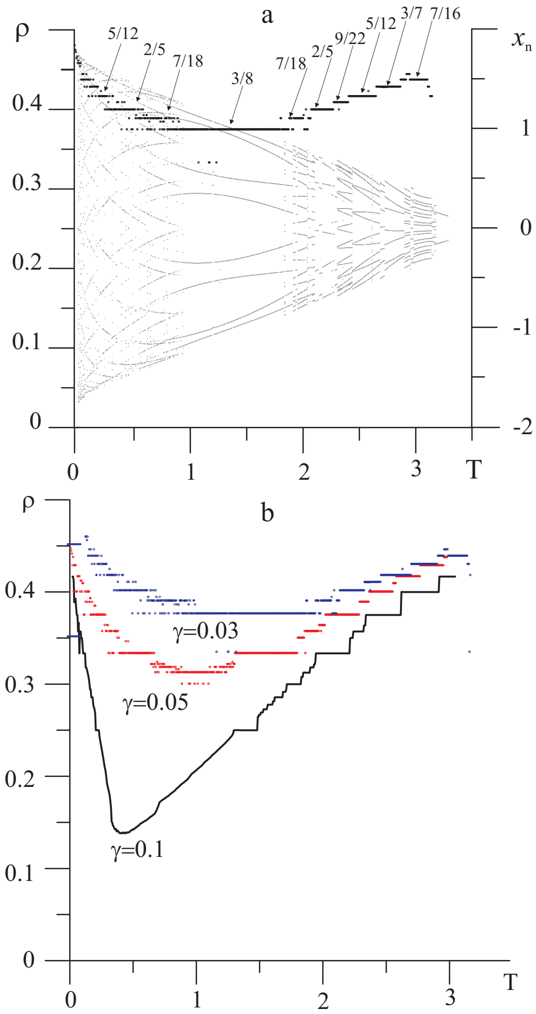

Fig. 13. Rotation number ρ as a function of the parameter T and bifurcation diagram (a) for the parameter values $\varepsilon = 0.005$, $\gamma = 0.03$. Plots of $\rho(T)$ at different values of the dissipation parameter γ (b).

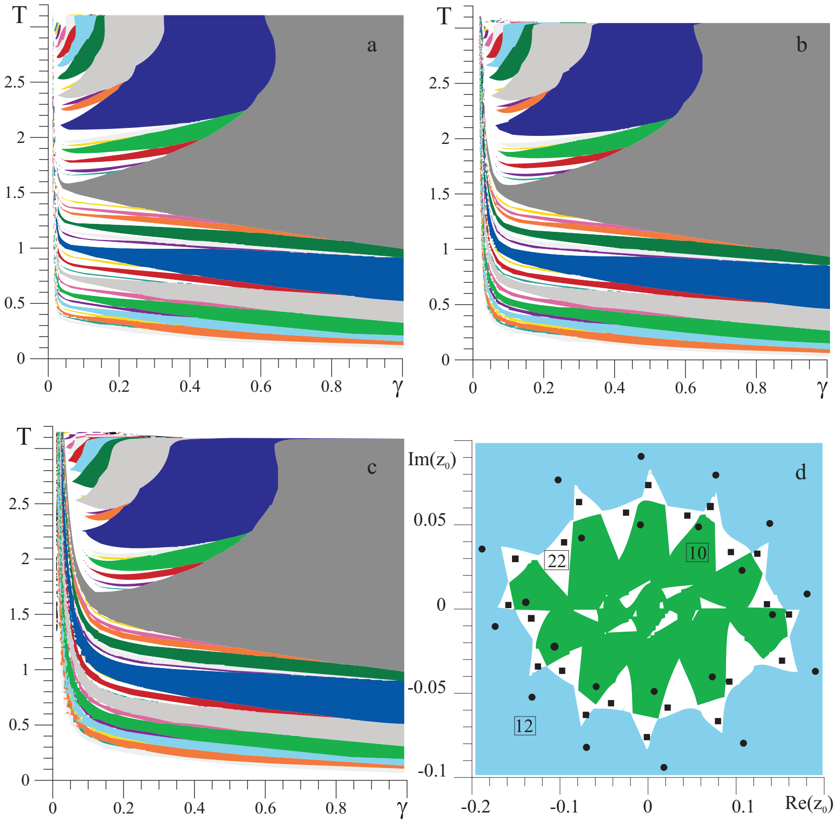

Fig. 14. Transformation of tongues of the map (16) with $3 \leq N \leq 16$ on the the parameter planes: $\varepsilon = -0.0001$ (nearly linear case) (a) , $\varepsilon = -0.001$ (b), $\varepsilon = -0.005$ (c). The case $\varepsilon \to 0$ corresponds to the plane depicted in Fig. 4. Coexisting limit cycles and their basins of attraction (d) for the parameter values $\varepsilon = -0.001$, $\gamma = 0.073$, $T = 2.78$. Depending on the starting conditions, trajectories approach either the 10-cycle (circles) with $\rho = 3/10$, the 12-cycle (circles) with $\rho = 5/12$ or the 22-cycle (squares) with $\rho = 9/22$.

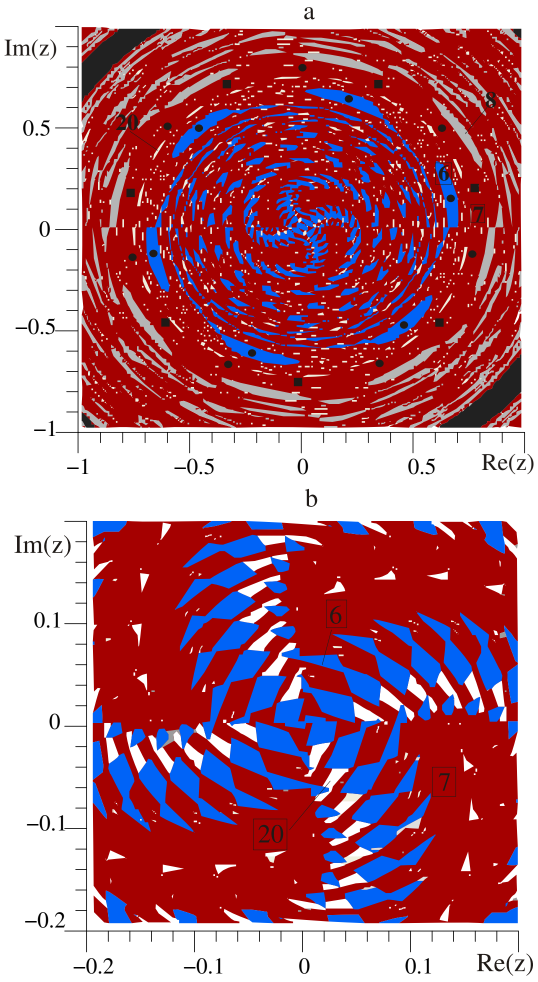

Fig. 15. Basins of attraction of coexisting limit cycles for the parameter values $\varepsilon = -0.001$, $\gamma = 0.02$, $T = 1.5$. Trajectories starting in different regions approach either one of the symmetric pair of 7-cycles with $\rho = 1/7$, the 6-cycle with $\rho = 1/6$, the 8-cycle with $\rho = 1/8$ or the 20-cycle with $\rho = 3/20$. Plot (b) is a fragment of (a).

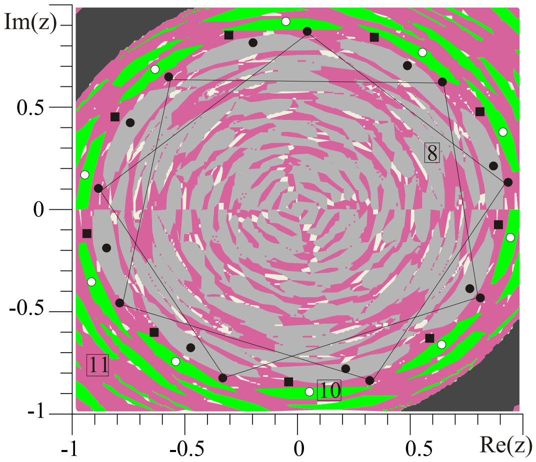

Fig. 16. Basins of attraction of coexisting limit cycles for the parameter values $\varepsilon = -0.005$, $\gamma = 0.03$, $T = 1.5$. Trajectories starting in different regions approach either the 8-cycle with $\rho = 1/8$, the 10-cycle with $\rho = 1/10$ or one of the symmetric pair of 11-cycle with $\rho = 1/11$.

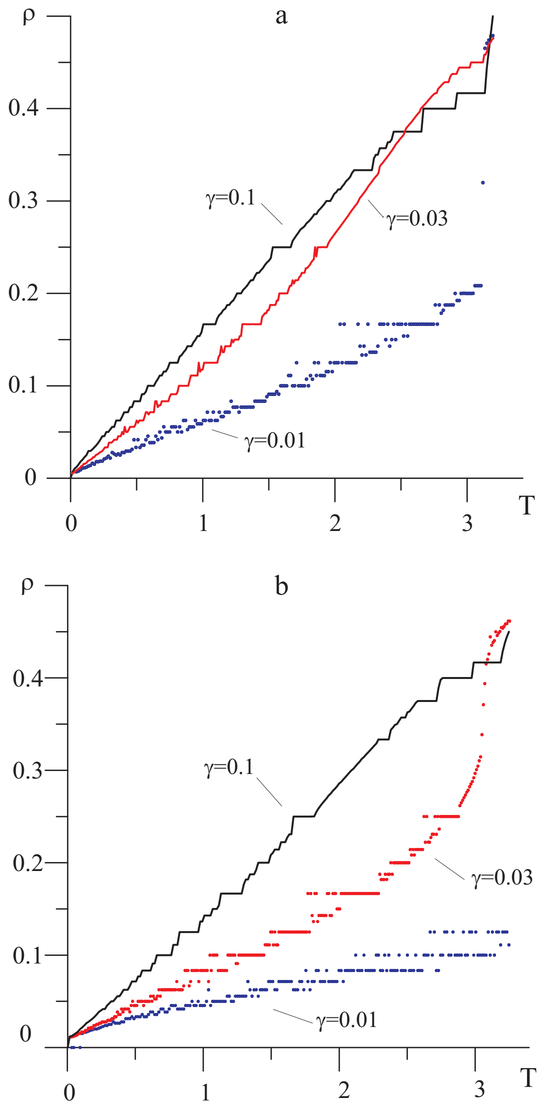

Fig. 17. Plots of $\rho(T)$ for the values of dissipation $\gamma = 0.01$, $\gamma = 0.03$, $\gamma = 0.1$. Plot (a) is calculated for $\varepsilon = -0.001$, (b) is for $\varepsilon = -0.005$.